

Stable Structural Analog of Ca^{2+} -ATPase ADP-insensitive Phosphoenzyme with Occluded Ca^{2+} Formed by Elongation of A-domain/M1'-linker and Beryllium Fluoride Binding^{*[5]}

Received for publication, May 13, 2010, and in revised form, May 30, 2010. Published, JBC Papers in Press, June 7, 2010, DOI 10.1074/jbc.M110.144535

Takashi Daiho¹, Stefania Danko, Kazuo Yamasaki, and Hiroshi Suzuki

From the Department of Biochemistry, Asahikawa Medical University, Asahikawa 078-8510, Japan

We have developed a stable analog for the ADP-insensitive phosphoenzyme intermediate with two occluded Ca^{2+} at the transport sites ($E2\text{PCa}_2$) of sarcoplasmic reticulum Ca^{2+} -ATPase. This is normally a transient intermediate state during phosphoenzyme isomerization from the ADP-sensitive to ADP-insensitive form and Ca^{2+} deocclusion/release to the lumen; $E1\text{PCa}_2 \rightarrow E2\text{PCa}_2 \rightarrow E2\text{P} + 2\text{Ca}^{2+}$. Stabilization was achieved by elongation of the Glu⁴⁰-Ser⁴⁸ loop linking the Actuator domain and M1 (1st transmembrane helix) with four glycine insertions at Gly⁴⁶/Lys⁴⁷ and by binding of beryllium fluoride (BeF_x) to the phosphorylation site of the Ca^{2+} -bound ATPase ($E1\text{Ca}_2$). The complex $E2\text{Ca}_2 \cdot \text{BeF}_3^-$ was also produced by luminal Ca^{2+} binding to $E2 \cdot \text{BeF}_3^-$ ($E2\text{P}$ ground state analog) of the elongated linker mutant. The complex was stable for at least 1 week at 25 °C. Only BeF_x , but not AlF_x or MgF_x , produced the $E2\text{PCa}_2$ structural analog. Complex formation required binding of Mg^{2+} , Mn^{2+} , or Ca^{2+} at the catalytic Mg^{2+} site. Results reveal that the phosphorylation product $E1\text{PCa}_2$ and the $E2\text{P}$ ground state (but not the transition states) become competent to produce the $E2\text{PCa}_2$ transient state during forward and reverse phosphoenzyme isomerization. Thus, isomerization and luminal Ca^{2+} release processes are strictly coupled with the formation of the acylphosphate covalent bond at the catalytic site. Results also demonstrate the critical structural roles of the Glu⁴⁰-Ser⁴⁸ linker and of Mg^{2+} at the catalytic site in these processes.

Sarcoplasmic reticulum Ca^{2+} -ATPase (SERCA1a)² catalyzes Ca^{2+} transport coupled with ATP hydrolysis (Fig. 1) (1–9). In the catalytic cycle the enzyme is activated by two cytoplasmic Ca^{2+} ions binding to the transport sites. It is then autophosphorylated at Asp³⁵¹ by MgATP to produce the ADP-sensitive

phosphoenzyme ($E1\text{P}$) that can react with ADP to regenerate ATP (steps 1–3). $E1\text{P}$ formation results in Ca^{2+} occlusion at the transport sites ($E1\text{PCa}_2$). Subsequent isomeric transition to an ADP-insensitive form ($E2\text{P}$), *i.e.* loss of ADP-sensitivity, results in Ca^{2+} deocclusion and release into the lumen (steps 4 and 5). This Ca^{2+} -release process is very rapid so that an $E2\text{PCa}_2$ intermediate state does not accumulate and in fact had never been found until we recently established its existence (10–13) and successfully trapped it for the first time (14). The Ca^{2+} -free $E2\text{P}$ is finally hydrolyzed to the inactive $E2$ state (steps 6 and 7). Mg^{2+} as the physiological catalytic cofactor is required for both phosphorylation and hydrolysis. The transport cycle is reversible. Thus, $E2\text{P}$ can be formed from P_i in the presence of Mg^{2+} and absence of Ca^{2+} . Subsequent Ca^{2+} binding to luminal-oriented low affinity transport sites reverses the Ca^{2+} -releasing step and the $E1\text{P}$ to $E2\text{P}$ isomerization.

During EP isomerization/ Ca^{2+} -release ($E1\text{PCa}_2 \rightarrow E2\text{P} + 2\text{Ca}^{2+}$), the A domain swings around parallel to the membrane plane (*i.e.* horizontal), whereas the A and P domains and M2 incline and tightly associate (Fig. 2) (15–25). We found that shortening of the A/M1'-linker by deletion of any single residue blocks $E1\text{PCa}_2 \rightarrow E2\text{PCa}_2$ isomerization and $E2\text{P}$ hydrolysis (26). On the other hand, its elongation by two or more glycine insertions markedly accelerates the isomerization and blocks Ca^{2+} deocclusion/release ($E2\text{PCa}_2 \rightarrow E2\text{P} + 2\text{Ca}^{2+}$) (14). Thus, elongating the A/M1'-linker stabilized the normally transient intermediate state $E2\text{PCa}_2$ (*i.e.* ADP-insensitive EP with occluded Ca^{2+}) and showed that the length of this linker is critical for the structural changes that occur during $E1\text{PCa}_2 \rightarrow E2\text{PCa}_2 \rightarrow E2\text{P} + 2\text{Ca}^{2+}$ and subsequent $E2\text{P}$ hydrolysis (14, 26).

We have recently developed an $E1\text{Ca}_2 \cdot \text{BeF}_3^-$ complex as a stable analog of $E1\text{PCa}_2 \cdot \text{Mg}^{2+}$ ($E1\text{PCa}_2$ with bound Mg^{2+} at the catalytic site) (27). Structural analysis of the analog and intermediate states suggests that formation of native $E1\text{PCa}_2 \cdot \text{Mg}^{2+}$ results in structural changes in the cytoplasmic and transmembrane domains due to configuration and ligation changes of the phosphate moiety (27). The Mg^{2+} bound at the catalytic site contributes to these structural changes (27). In fact, Ca^{2+} could not substitute for Mg^{2+} for formation of $E1\text{Ca}_2 \cdot \text{BeF}_3^-$, and an attempt to substitute Ca^{2+} for Mg^{2+} destroyed the complex (27). It is well known that Ca^{2+} substitution of Mg^{2+} at the catalytic site markedly retards $E1\text{PCa}_2 \cdot \text{Ca}$ isomerization (28, 29), a step that includes rotation of the A domain.

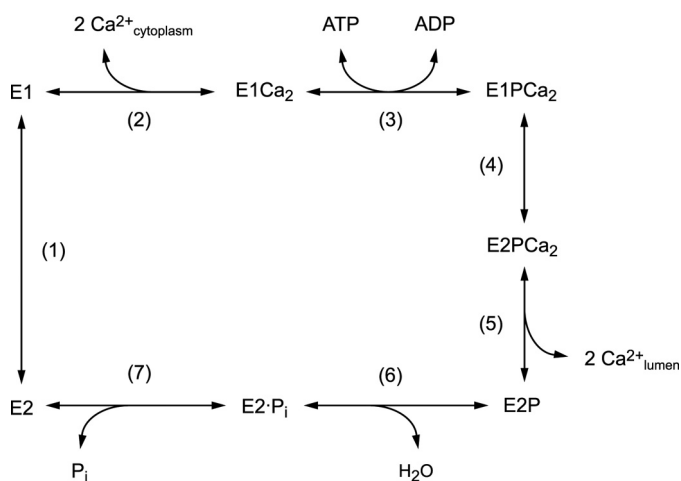
Further understanding of the mechanism of EP processing via the transient $E2\text{PCa}_2$ and of the critical roles of the A/M1'-

* This work was supported by a grant-in-aid for Scientific Research (C) (to T. D.) and (B) (to H. S.) from the Ministry of Education, Culture, Sports, Science, and Technology of Japan.

[5] The on-line version of this article (available at <http://www.jbc.org>) contains supplemental Figs. S1–S6 and Tables S1 and S2.

¹ To whom correspondence should be addressed: Dept. of Biochemistry, Asahikawa Medical University, Midorigaoka-higashi, Asahikawa, 078-8510, Japan. Tel.: 81-166-68-2353; Fax: 81-166-68-2359; E-mail: daiho@asahikawa-med.ac.jp.

² The abbreviations used are: SERCA1a, adult fast-twitch skeletal muscle sarcoplasmic reticulum Ca^{2+} -ATPase; EP , phosphoenzyme; $E1\text{PCa}_2$, ADP-sensitive phosphoenzyme with occluded Ca^{2+} ; $E2\text{PCa}_2$, ADP-insensitive phosphoenzyme with occluded Ca^{2+} ; $E2\text{P}$, ADP-insensitive phosphoenzyme; TG, thapsigargin; MOPS, 3-(*N*-morpholino)propanesulfonic acid; prtK, proteinase K; AMPPCP, adenosine 5'-(β , γ -methylene)triphosphate.

FIGURE 1. Ca²⁺-transport cycle of SERCA.

linker and catalytic Mg²⁺ requires detailed characterization of the development of E2PCa₂ and of factors contributing to its possible stabilization. A great advance would be the finding of an analog stable enough for crystallographic studies.

In this study we employed the mutant 4Gi-46/47 in which the A/M1'-linker is elongated by four glycine insertions at Gly⁴⁶/Lys⁴⁷ (14) and explored the formation of a stable structural analog of E2PCa₂ using various configuration analogs of phosphate (BeF_x/AlF_x/MgF_x) and catalytic cations (Mg²⁺/Mn²⁺/Ca²⁺). We found that BeF_x is uniquely efficacious and that both mutant E1Ca₂·BeF₃⁻ and mutant E2·BeF₃⁻ are capable of producing mutant E2Ca₂·BeF_x, most probably E2Ca₂·BeF₃⁻, and that Ca²⁺ can replace the catalytic Mg²⁺ when coming from the former species. The mutant complex E2Ca₂·BeF₃⁻ is extremely stable even at 25 °C.

EXPERIMENTAL PROCEDURES

Mutagenesis and Expression—The pMT2 expression vector (30) carrying the mutant rabbit SERCA1a cDNA with four glycine residues inserted between Gly⁴⁶ and Lys⁴⁷ (4Gi-46/47) was constructed as described previously (14). Transfection of pMT2 DNA into COS-1 cells and preparation of microsomes from the cells were performed as described previously (31). The amount of expressed SERCA1a was quantified by a sandwich enzyme-linked immunosorbent assay (32). Expression levels of wild type SERCA1a and the mutants were 2–3% that of total microsomal proteins.

Metal Fluoride Treatment—Microsomes expressing the wild type or 4Gi-46/47 were treated at 25 °C for 30 min with BeF_x, AlF_x, and MgF₄²⁻ as described previously (14, 23–25, 27, 33–36) and in the legends for Figs. 3–9 in detail.

Formation of EP—Phosphorylation of SERCA1a in microsomes with [³²P]ATP was performed under conditions described in the legends for Figs. 3–8. The reactions were quenched with ice-cold trichloroacetic acid containing P_i. Precipitated proteins were separated by 5% SDS-PAGE at pH 6.0 according to Weber and Osborn (37). The radioactivity associated with the separated Ca²⁺-ATPase was quantified by digital autoradiography as described (38).

Ca²⁺ Occlusion in SERCA1a—Microsomes treated with metal fluoride were diluted with “washing solution” contain-

ing excess EGTA and then immediately filtered through a 0.45- μ m nitrocellulose membrane filter (Millipore). The filter was washed extensively with the washing solution, and ⁴⁵Ca²⁺ remaining on the filter was quantified. The amount of Ca²⁺ specifically bound to the transport sites of EP in the expressed SERCA1a was obtained by subtracting the amount of nonspecific Ca²⁺-binding, which was determined as described in the legends for Figs. 8 and 9. The Ca²⁺ occluded/mg of expressed SERCA1a protein was calculated from the amount of expressed SERCA1a and the amount of occluded Ca²⁺.

Limited Proteolysis and Western Blot Analysis—Major intermediates of the Ca²⁺-ATPase and their stable analogs were produced and subjected to structural analysis by limited proteolysis with trypsin and proteinase K (prtK) as described in the legends for supplemental Figs. S3 and S4. Proteolysis was terminated by 2.5% (v/v) trichloroacetic acid. The digests were subjected to SDS-PAGE (39) followed by Western blot analysis with IH11 monoclonal antibody to the rabbit SERCA1a (Affinity Bioreagents), which recognizes an epitope between Ala¹⁹⁹ and Arg⁵⁰⁵ as described (14).

Miscellaneous—Protein concentrations were determined by the method of Lowry *et al.* (40) with bovine serum albumin as a standard. Data were analyzed by nonlinear regression using the program Origin (Microcal Software, Inc., Northampton, MA). Three-dimensional models of the enzyme were reproduced by the program VMD (41).

RESULTS

Inhibition of EP Formation by Metal Fluoride—The E1Ca₂ state of wild type and mutant 4Gi-46/47 SERCA1a in 10 μ M Ca²⁺ was treated with BeF_x or AlF_x and functionally analyzed. The ability to form EP from ATP (Fig. 3, A and C) and from P_i (data not shown) is almost completely lost in the presence of 15 mM Mg²⁺ but not in its absence. EP formation is not inhibited when F⁻ treatment in 15 mM Mg²⁺ is made without Be²⁺ or Al³⁺. The results show that the E1Ca₂ state of the mutant as well as of wild type forms stable complexes with BeF_x and AlF_x in the presence of Mg²⁺ but not with MgF_x.

When the E2 state of wild type and mutant 4Gi-46/47 in the absence of Ca²⁺ was treated with BeF_x, AlF_x, and MgF_x (in the absence of Be²⁺ and Al³⁺), the complexes E2·BeF₃⁻, E2·AlF₄⁻, and E2·MgF₄²⁻, respectively, are produced (14, 25), and EP formation from ATP (Fig. 3, B and D, *open bars*) and from P_i (data not shown) is almost completely inhibited. These complexes were then treated with 10 mM Ca²⁺ for 1 h in the presence of Ca²⁺ ionophore A23187 (*black bars* in Fig. 3, B and D). In the case of wild type, the ability to form EP is restored, consistent with the previous observation (25, 36) that a high concentration of Ca²⁺ in the presence of A23187 restores Ca²⁺-ATPase activity by destroying the complexes and converting the enzyme to E1Ca₂. In mutant 4Gi-46/47, the Ca²⁺-induced restoration of EP formation is observed with E2·MgF₄²⁻ and E2·AlF₄⁻ but not at all with E2·BeF₃⁻. E2·BeF₃⁻ of the mutant is, thus, resistant to Ca²⁺. We previously found (14) that the transient intermediate E2PCa₂ is produced and trapped in the mutant in the reverse direction of the pump cycle from E2P by Ca²⁺ binding from the luminal side as well as in the forward direction from E1Ca₂ through

Stable Analog of Transient E2P with Occluded Ca^{2+} in SERCA

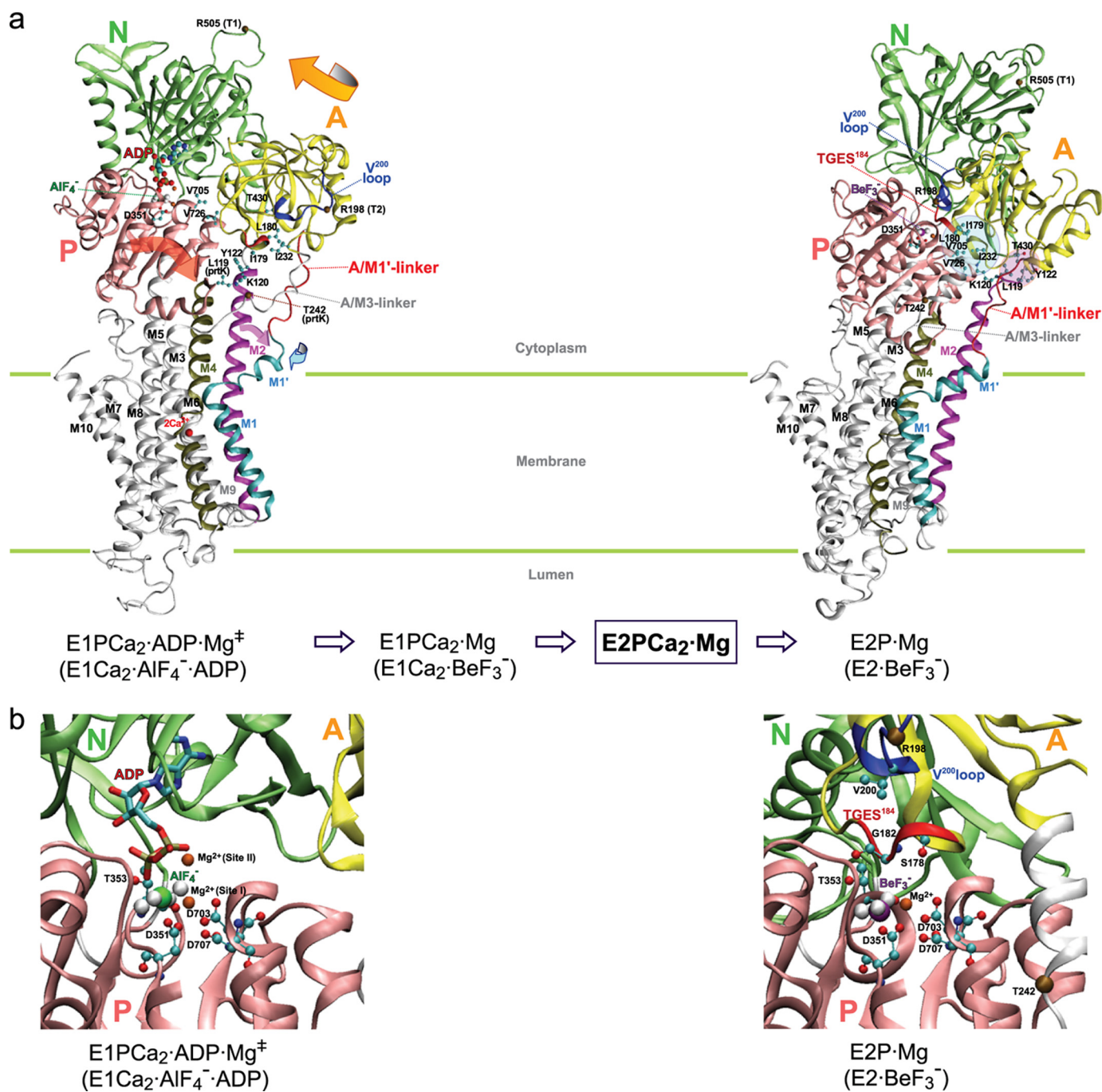


FIGURE 2. Crystal structures of SERCA1a. The coordinates for structures $\text{E1Ca}_2 \cdot \text{AlF}_4^- \cdot \text{ADP}$ (the analog of the transition state of phosphorylation, *left*) and $\text{E2} \cdot \text{BeF}_3^-$ (the analog of the E2P ground state, *right*) were obtained from Protein Data Bank (PDB accession code 1T5T (17) and 2ZBE (21), respectively). *a*, the cytoplasmic domains N (nucleotide binding), P (phosphorylation), A (actuator), 10 transmembrane helices (M1–M10), phosphorylation site Asp³⁵¹, and TGES¹⁸⁴ on the A domain are indicated. Cleavage sites by trypsin (T1 (Arg⁵⁰⁵) and T2 (Arg¹⁹⁸ on the Val²⁰⁰ loop (DPRV\NQD²⁰³)) and by prtK (Leu¹¹⁹ on the top part of M2 and Thr²⁴² on the A/M3-linker) are shown. *Arrows* indicate approximate motions of the A and P domains, M2, and M1' from $\text{E1Ca}_2 \cdot \text{AlF}_4^- \cdot \text{ADP}$ to $\text{E2} \cdot \text{BeF}_3^-$. Note the large rotation of the A domain and the inclination of the P and A domains and M2. In the E2P state the A and P domains interact at three regions; at the ¹⁸¹TGES loop with the residues around Asp³⁵¹, at the Val²⁰⁰ loop (Asp¹⁹⁶-Asp²⁰³) with polar residues of the P domain, and at Leu¹¹⁹/Tyr¹²² on the top part of M2 with the A, P, and N domains. In $\text{E2} \cdot \text{BeF}_3^-$ (TG) (PDB accession code 2ZBF (21), [supplemental Fig. S5](#)), Leu¹¹⁹/Tyr¹²² produce the Tyr¹²²-hydrophobic cluster with five other hydrophobic residues, Ile¹⁷⁹/Leu¹⁸⁰/Ile²³² of the A domain and Val⁷⁰⁵/Val⁷²⁶ of the P domain. In $\text{E2} \cdot \text{BeF}_3^-$ without TG, the cluster structure is rather loose (as the side chains of Leu¹¹⁹/Tyr¹²² are pointing away from the hydrophobic cluster), but Leu¹¹⁹/Tyr¹²² produce a more extended interaction network involving Thr⁴³⁰ of the N domain and the hydrophobic cluster (see more details in [supplemental Fig. S5](#)). *b*, the catalytic site is enlarged, and the residues involved in the Mg²⁺ (site I) are depicted. The Val⁶⁷⁹-Lys⁶⁸⁶ region of the P domain is not depicted for simplicity (because it is positioned over the region of interest).

ATP-induced phosphorylation. Therefore, the complex produced in the mutant with BeF_x is likely $\text{E2Ca}_2 \cdot \text{BeF}_3^-$, an analog of E2PCa_2 (as is in fact shown later in the Ca^{2+} binding and structural analyses in Fig. 8 and [supplemental Figs. S3 and S4](#)).

Kinetic Analysis of BeF_x -induced Complex Formation—The E1Ca_2 state of mutant 4Gi-46/47 was treated with various concentrations of Be^{2+} and 1 mM F^- in 10 μM Ca^{2+} and 15 mM Mg^{2+} , and the resulting species was analyzed (Fig. 4A). The

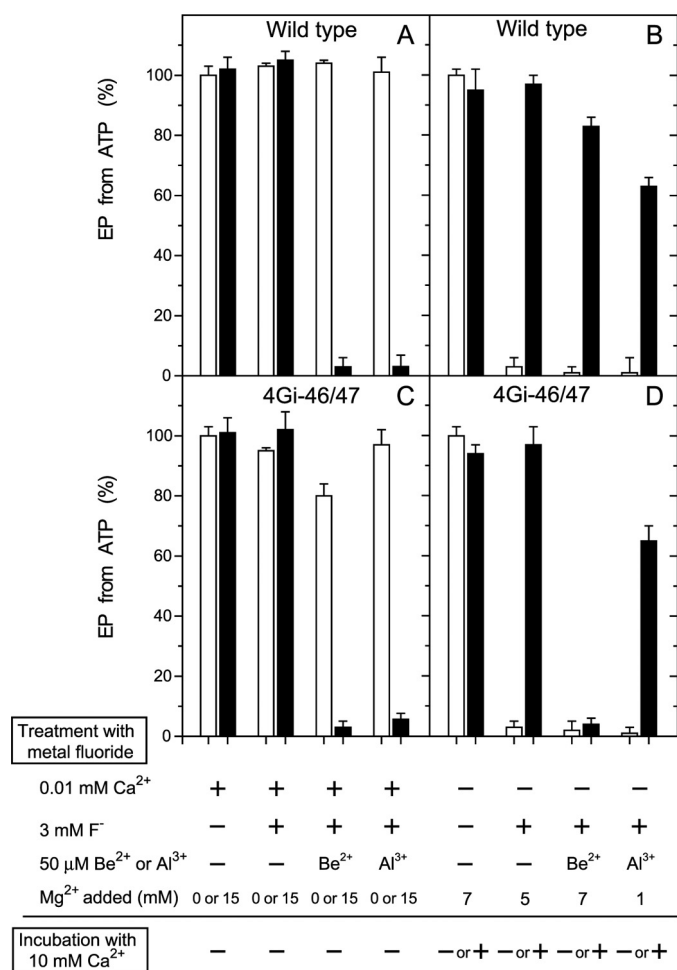


FIGURE 3. Inhibition of EP formation from ATP by metal fluoride. A and C, microsomes expressing the wild type or mutant 4Gi-46/47 (0.35 mg/ml) were treated at 25 °C for 30 min with metal fluoride in the presence of 0.01 mM Ca²⁺ (0.01 mM CaCl₂ without EGTA) in 3 mM KF plus 50 μM BeSO₄ or AlCl₃, 0.1 M KCl, and 50 mM MOPS/Tris (pH 7) with (black bar) or without (white bar) 15 mM MgCl₂. Subsequently, the samples were diluted 10-fold and phosphorylated at 0 °C for 15 s with 10 μM [³²P]ATP in 1 μM A23187, 0.1 mM Ca²⁺ (0.5 mM CaCl₂ with 0.4 mM EGTA), 7 mM MgCl₂, 0.1 M KCl, and 50 mM MOPS/Tris (pH 7), and the amount of EP formed was determined. The amount of EP formed with the wild type in the control sample, *i.e.* incubated without the fluoride compounds and Mg²⁺ (4.7 nmol/mg of the expressed SERCA1a), was normalized to 100%. The amount of EP formed with the mutant 4Gi-46/47 in the control sample was almost the same as that of wild type. B and D, microsomes were treated with metal fluoride in the absence of Ca²⁺ (1 mM EGTA without added CaCl₂) and in the presence of the indicated concentrations of MgCl₂. Subsequently, the samples were diluted 2.5-fold with a solution containing 1 μM A23187, 0.1 M KCl, 50 mM MOPS/Tris (pH 7), and EGTA (to give 1 mM, white bar) or CaCl₂ (to give 10 mM Ca²⁺, black bar) and incubated at 25 °C for 1 h. The samples were then further diluted 10-fold and phosphorylated with 10 μM [³²P]ATP and 0.1 mM Ca²⁺ as in A and C, and the amount of EP formed was determined.

presence of both Be²⁺ and F⁻ (BeF_x) but not F⁻ without Be²⁺ or Be²⁺ (20 μM) without F⁻ inhibits EP formation. The time courses of BeF_x-induced inhibition follow first order kinetics. A plot of the inhibition rate constants *versus* Be²⁺ (BeF_x) concentration is a straight line with no evidence of saturation within the experimental range, indicating that BeF_x binding is the rate-determining step in the inhibition process (Fig. 4B). BeF_x inhibits wild type at nearly the same rate as it does the mutant as seen at a representative 20 μM Be²⁺ with 1 mM F⁻.

In Fig. 5, the mutant E1Ca₂ state in 10 μM Ca²⁺ was incubated with BeF_x at various Mg²⁺ concentrations, and the level

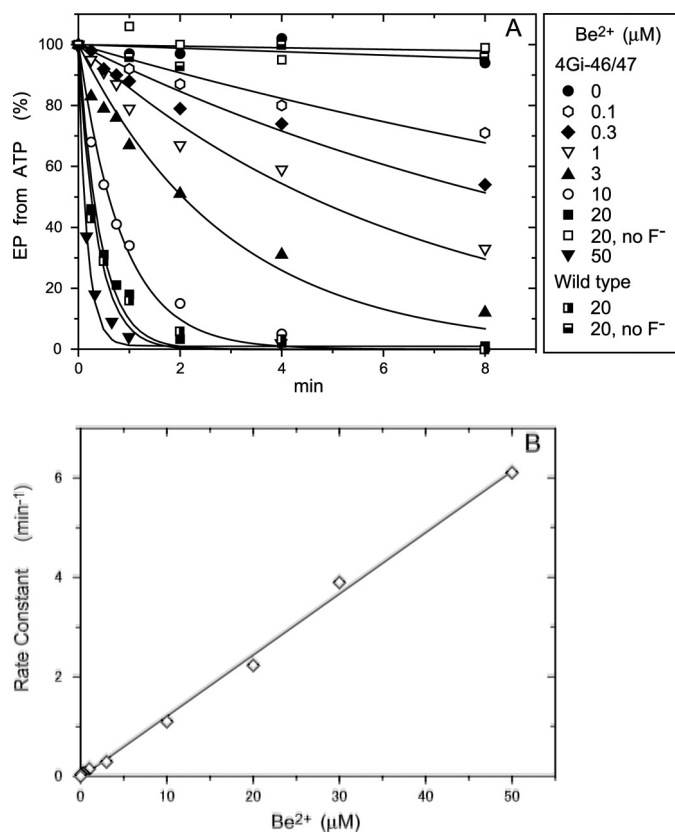


FIGURE 4. Be²⁺ dependence of the rate of EP inhibition by BeF_x in 0.01 mM Ca²⁺. A, microsomes expressing the wild type or mutant 4Gi-46/47 were incubated for various periods in 0.01 mM Ca²⁺ and 1 mM KF with various concentrations of BeSO₄ and otherwise as in Fig. 3, A and C, for BeF_x-treatment. The samples were then diluted 10-fold and phosphorylated with 10 μM [³²P]ATP, and the amount of EP formed was determined, as in Fig. 3, A and C. Solid lines show the least squares fit to a single exponential. In B, the rate constants obtained in A were plotted *versus* the concentration of Be²⁺ added. The linear fit to the data gave a slope of 0.123 min⁻¹μM⁻¹.

of inhibition of EP formation was determined. BeF_x-induced inhibition is markedly accelerated with increasing Mg²⁺, giving a K_{0.5} value of 4.9 mM. The observed apparent Mg²⁺ affinity is consistent with those values obtained through phosphorylation of native Ca²⁺-ATPase (42–47) and for the formation of E1Ca₂·BeF₃⁻ (E1PCa₂·Mg²⁺ analog) (27), *i.e.* the Mg²⁺ binding affinity at the catalytic Mg²⁺ site (site I composed of Asp³⁵¹/Thr³⁵³/Asp⁷⁰³ and the phosphate moiety (BeF₃⁻)). Therefore, Mg²⁺ binding at site I is likely a prerequisite for BeF_x binding and complex formation.

In Figs. 6 and 7, we further observed that the BeF_x-induced complex formation from E1Ca₂ in the mutant occurs with Mn²⁺ or Ca²⁺ in place of Mg²⁺. The K_{0.5} values are 1.4 mM for Mn²⁺ and 0.76 mM for Ca²⁺ (supplemental Figs. S1 and S2) and are consistent with such values for binding to the catalytic Mg²⁺ site (46, 48). In wild type the BeF_x-induced E1Ca₂·BeF₃⁻ formation, which inhibits EP formation occurs with Mn²⁺ but not with 10 mM Ca²⁺ in place of Mg²⁺ (Figs. 6 and 7). Thus, the complex formed from E1Ca₂ with BeF_x in the mutant 4Gi-46/47 (*i.e.* E2Ca₂·BeF₃⁻) is distinct from E1Ca₂·BeF₃⁻ of wild type.

Interestingly, the Hill coefficient for the Mg²⁺ as well as Mn²⁺ and Ca²⁺ dependence for complex formation with BeF_x (E2Ca₂·BeF₃⁻) in the mutant is nearly 2 (Fig. 5 and supplemental Figs. S1 and S2), suggesting the involvement of more

Stable Analog of Transient E2P with Occluded Ca²⁺ in SERCA

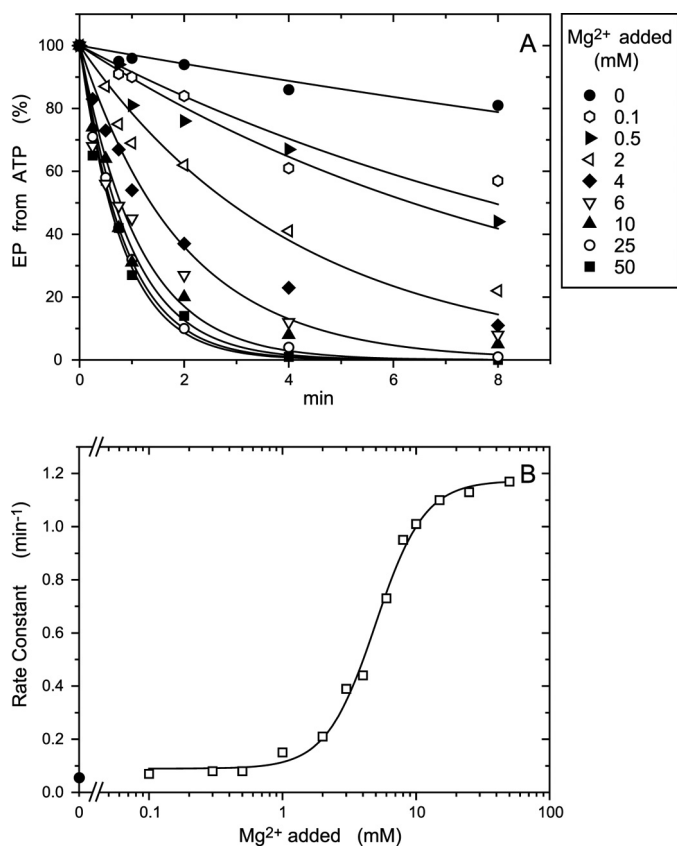


FIGURE 5. Mg²⁺ dependence of the rate of EP inhibition by Be_x in 0.01 mM Ca²⁺. A, microsomes expressing the mutant 4Gi-46/47 were incubated for various periods in 0.01 mM Ca²⁺, 1 mM KF, 10 μM BeSO₄, and various concentrations of MgCl₂ and otherwise as in Fig. 3, A and C, for Be_x treatment. The samples were then diluted 10-fold and phosphorylated with 10 μM [^γ-³²P]ATP, and the amount of EP formed was determined, as in Fig. 3, A and C. Solid lines show the least squares fit to a single exponential. In B the rate constants obtained in A were plotted versus the concentration of Mg²⁺ added. K_{0.5} for the Mg²⁺ activation and Hill coefficient obtained by fitting to the Hill equation (solid line) were 4.9 mM and 2.3, respectively.

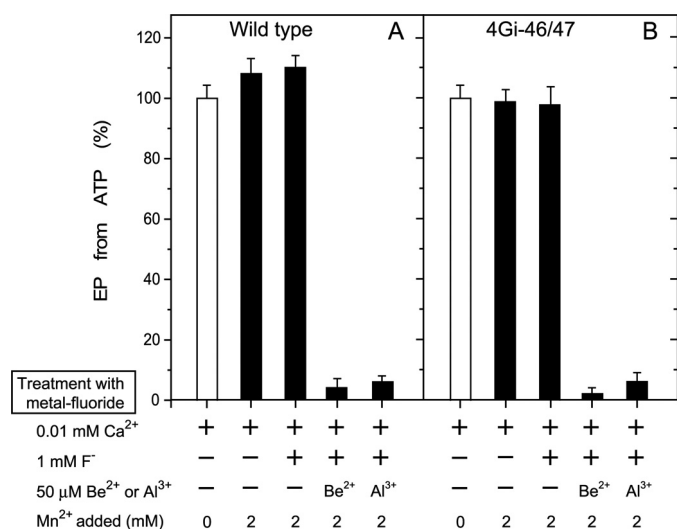


FIGURE 6. EP inhibition by Mn²⁺ and Be_x in 0.01 mM Ca²⁺ without Mg²⁺. Microsomes expressing the wild type or mutant 4Gi-46/47 were treated with 1 mM F⁻ plus 50 μM Be²⁺ or Al³⁺ in 0.01 mM Ca²⁺ and in the absence (white bar) or presence (black bar) of 2 mM MnCl₂ (in place of MgCl₂) and otherwise as in Fig. 3, A and C. The samples were then diluted 10-fold and phosphorylated with 10 μM [^γ-³²P]ATP, and the amount of EP formed was determined as in Fig. 3, A and C.

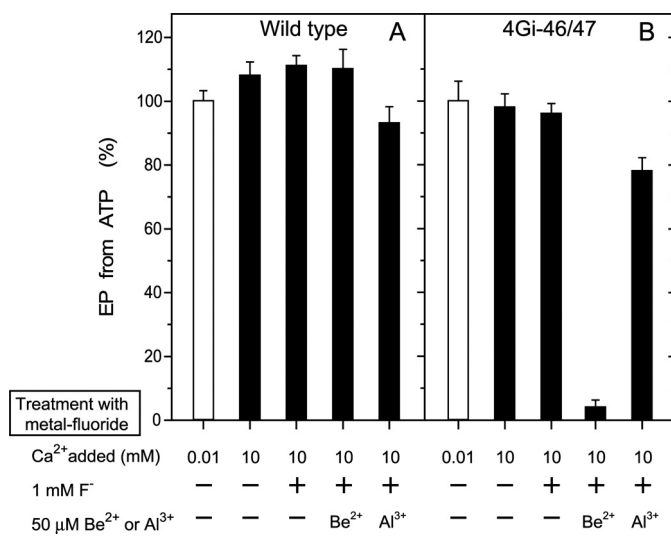


FIGURE 7. EP inhibition by 10 mM Ca²⁺ and Be_x without Mg²⁺ and Mn²⁺. Microsomes expressing wild type or mutant 4Gi-46/47 were treated with 1 mM F⁻ plus 50 μM Be²⁺ or Al³⁺ in 0.01 or 10 mM CaCl₂ without Mg²⁺ and Mn²⁺ and otherwise as in Fig. 3, A and C. The samples were then diluted 10-fold and phosphorylated with 10 μM [^γ-³²P]ATP, and the amount of EP was determined as in Fig. 3, A and C.

than one metal ion. This is in contrast to the value 1 for E1Ca₂·BeF₃⁻ formation with Mg²⁺ and Mn²⁺ in wild type (see supplemental Fig. 1 in Ref. 27).

AlF_x produces the complex with the E1Ca₂ state of the mutant 4Gi-46/47 as well as of wild type (E1Ca₂·AlF_x) with Mg²⁺ and Mn²⁺ but not with Ca²⁺ at the catalytic Mg²⁺ site (Figs. 3, 6, and 7). Therefore, in the mutant the complex with AlF_x (E1Ca₂·AlF_x) is distinct from that with BeF_x (E2Ca₂·BeF₃⁻) with respect to the strict preference of the divalent cation at the catalytic Mg²⁺ site.

Ca²⁺ Occlusion in the Mutant Complexed with BeF_x.—In Fig. 8A, the E1Ca₂ state of the mutant 4Gi-46/47 in 10 μM ⁴⁵Ca²⁺ and 15 mM Mg²⁺ was complexed with BeF_x at a low concentration of Be²⁺ (1 μM) with 1 mM F⁻ to slow complex formation. The amount of occluded ⁴⁵Ca²⁺ was determined at various periods by membrane filtration with extensive washing with a solution containing excess EGTA and A23187. The loss of EP-forming ability with ATP decreases reciprocally and linearly with an increase in the amount of occluded Ca²⁺ (see the inset). The amount of occluded ⁴⁵Ca²⁺ at the intercept of the abscissa, i.e. when all the ATPases are complexed with BeF_x, is 8.4 nmol/mg of expressed SERCA1a mutant protein. The stoichiometry of the occluded Ca²⁺ is nearly 2 per phosphorylation site, which is 4.3 nmol/mg as determined from the intercept on the ordinate. Therefore, the complex formed with BeF_x has two occluded Ca²⁺. When the mutant was incubated for 15 min with BeF_x and 1.5 mM Mn²⁺ in place of Mg²⁺ under otherwise identical conditions, EP formation was completely inhibited, and the amount of occluded ⁴⁵Ca²⁺ was 8.3 nmol/mg of expressed SERCA1a mutant protein, giving a stoichiometry of 2 per phosphorylation site (data not shown).

In Fig. 8B, we examined whether the complex E2Ca₂·BeF₃⁻ can be produced from E2·BeF₃⁻ by luminal Ca²⁺ binding, mimicking the reverse conversion E2P + 2Ca²⁺ → E2PCa₂ (14). E2·BeF₃⁻ was first formed in the mutant in the absence of Ca²⁺

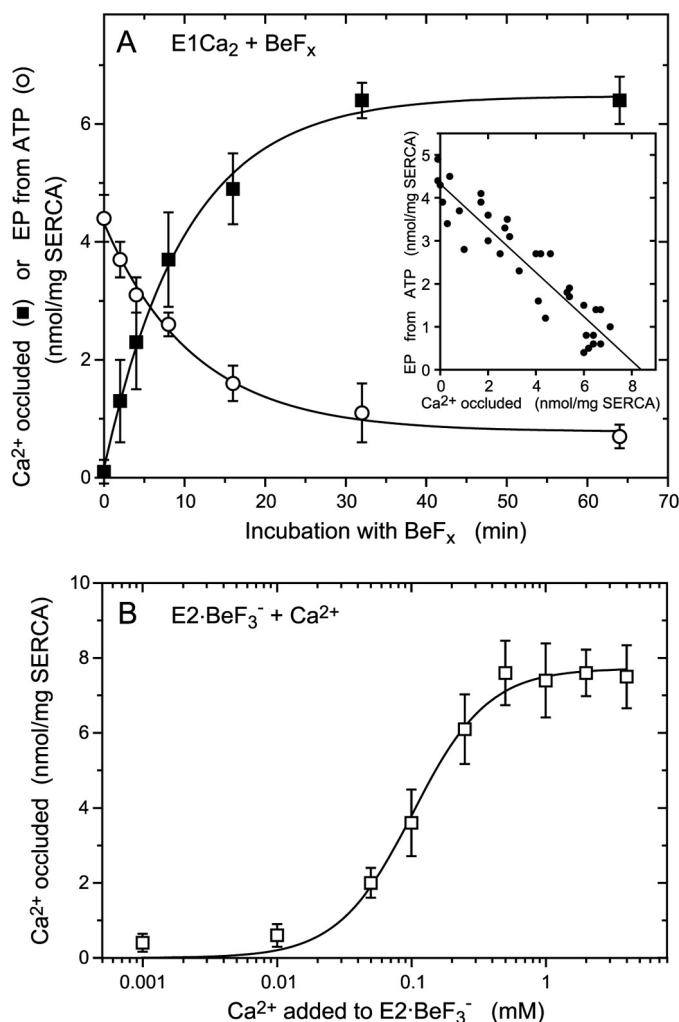


FIGURE 8. Ca²⁺ occlusion in E2Ca₂·BeF₃⁻ of the mutant 4Gi-46/47 formed from E1Ca₂ (A) and from E2·BeF₃⁻ (B). A, microsomes (0.2 mg/ml) expressing the mutant 4Gi-46/47 were incubated for various periods at 25 °C in 10 μl of a mixture containing 0.01 mM ⁴⁵CaCl₂, 1 mM KF, 1 μM BeSO₄, 15 mM MgCl₂, 0.1 M KCl, 50 mM MOPS/Tris (pH 7). The mixture was then diluted 200-fold at 0 °C with a washing solution containing 2 mM EGTA, 5 μM A23187, 0.1 M KCl, 7 mM MgCl₂, and 50 mM MOPS/Tris (pH 7.0), subjected to membrane filtration, and washed rapidly with 6 ml of the washing solution for 4 s at 0 °C. For determination of EP, the above BeF_x-incubation was made with ⁴⁰Ca²⁺ instead of ⁴⁵Ca²⁺ otherwise as above, and the sample was diluted 10-fold and phosphorylated with 10 μM [γ-³²P]ATP at 0 °C for 15 s as in Fig. 3C. The sample was then further diluted 20-fold at 0 °C with the washing solution, immediately filtered as above, and washed rapidly with ice-cold trichloroacetic acid containing P_i. The EP level was not changed during the above sample handling because the decay of EP (E2PCa₂) is almost completely blocked in the mutant (14). The amount of ⁴⁵Ca²⁺ specifically bound and occluded (■) and that of E³²P formed (○) in the expressed SERCA1a mutant were obtained by subtracting the background levels determined by including 1 μM TG in the BeF_x incubation mixture. The values presented are the mean ± S.D. (n = 5). *Inset*, the amount of EP formed was replotted versus that of occluded Ca²⁺ with the BeF_x treatment. The solid line represents the linear least squares fit. The y and x intercepts gave 4.3 and 8.4 nmol/mg of the expressed SERCA1a for the amounts of EP and of Ca²⁺ occluded, respectively. B, for formation of E2·BeF₃⁻, microsomes (1 mg/ml) expressing the mutant 4Gi-46/47 were incubated at 25 °C for 30 min with 1 mM KF and 20 μM BeSO₄ in 1 mM EGTA, 7 mM MgCl₂, 50 mM LiCl, and 50 mM MOPS/Tris (pH 7). Then the mixture was diluted 2.5-fold with a solution containing 7 mM MgCl₂, 50 mM LiCl, 50 mM MOPS/Tris (pH 7), 5 μM Ca²⁺ ionophore A23187, and various concentrations of ⁴⁵CaCl₂ to give the indicated final ⁴⁵Ca²⁺ concentrations. After incubating at 25 °C for 1 min, the mixture was further diluted with 400-fold of the washing solution containing the excess EGTA, filtered, and washed with the washing solution as above. The amount of ⁴⁵Ca²⁺ specifically bound and occluded in the SERCA1a was obtained by subtracting the nonspecific Ca²⁺ binding, which was determined without KF in the BeF_x treatment

and then incubated for 1 min at 25 °C with various concentrations of ⁴⁵Ca²⁺ in the presence of Ca²⁺ ionophore A23187. The amount of occluded ⁴⁵Ca²⁺ was determined after a large dilution followed by filtration and extensive EGTA washing. The maximum amount of occluded ⁴⁵Ca²⁺ is 7.7 nmol/mg of mutant SERCA1a protein and 1.8 times that of the phosphorylation site (4.3 nmol/mg), giving a stoichiometry of nearly 2. Thus, mutant E2Ca₂·BeF₃⁻ is produced from mutant E2·BeF₃⁻ by the addition of Ca²⁺ in the presence of A23187.

*K*_{0.5} and the Hill coefficient observed in Fig. 8B are 0.1 mM and ~2, respectively, *i.e.* very similar values to those observed during E2PCa₂ formation from E2P and Ca²⁺ in the mutant (14). The observed low Ca²⁺ affinity is in agreement with the wild type property (25, 49) that E2·BeF₃⁻ as well as E2P have low affinity Ca²⁺ binding sites; that is, the luminal-oriented transport sites. Importantly, E2Ca₂·BeF₃⁻/E2PCa₂ formed in the mutant (either from E1Ca₂ or from E2·BeF₃⁻/E2P) is remarkably stable and virtually not in equilibrium with E1Ca₂·BeF₃⁻/E1PCa₂ or E2·BeF₃⁻/E2P, *i.e.* their formation is almost irreversible, as shown previously (14) and in this study. When Ca²⁺ comes from the cytoplasmic side for E2PCa₂ formation from E1Ca₂ with ATP (via E2 → E1Ca₂ → E1PCa₂ → E2PCa₂) in the mutant, the apparent Ca²⁺ affinity is very high, with *K*_{0.5} = 0.14 μM (14), equal to the value for cytoplasmic Ca²⁺ binding at the transport sites in wild type. Also in the case of mutant E2Ca₂·BeF₃⁻ formation from E1Ca₂ with BeF_x in Fig. 8A, 10 μM Ca²⁺ is obviously enough to saturate (even 1 μM Ca²⁺ saturates (data not shown)), suggesting a similar high Ca²⁺ affinity as in E2PCa₂ formation from E1 + 2Ca²⁺.

Structures of Complexes Formed from E1Ca₂ with Metal Fluoride—During the Ca²⁺ transport cycle, the A, P, and N domains move and reorganize substantially. These changes can be monitored by proteolytic patterns and resistance against trypsin and prtK (23, 24). Therefore, we applied proteolytic analyses to mutant E2Ca₂·BeF₃⁻ to reveal the position of the domains and to establish whether it is a true structural E2PCa₂ analog (supplemental Figs. S3 and S4 and Tables S1 and S2 and Refs. 54 and 55). All the various major intermediates and their analogs were formed from E1Ca₂ in the mutant and wild type and then subjected to proteolyses. The results show that mutant E2Ca₂·BeF₃⁻ has the same structure as that of mutant E2PCa₂ and that this structural state is intermediate between wild type E1PCa₂ (wild type E1Ca₂·BeF₃⁻) and Ca²⁺-free E2P (wild type as well as mutant E2·BeF₃⁻) as described below. In mutant E2Ca₂·BeF₃⁻ and in mutant E2PCa₂, the T2 site Arg¹⁹⁸ on the Val²⁰⁰ loop is completely resistant to trypsin, as in wild type E2P (E2·BeF₃⁻), showing that the A domain has rotated from its position in E1PCa₂ (E1Ca₂·BeF₃⁻ of wild type) and is associated with the P domain at Arg¹⁹⁸ of the Val²⁰⁰ loop.

In both wild type E1Ca₂·BeF₃⁻ (E1PCa₂) and wild type and mutant E2·BeF₃⁻ (E2P), Leu¹¹⁹ on the upper portion of M2 is completely resistant to prtK attack and is, thus, sterically protected as found previously (Refs. 25 and 27; see a detailed

mixture. In fitting to the Hill equation (solid line), the maximum amount of occluded Ca²⁺, *K*_{0.5} for the Ca²⁺ activation, and Hill coefficient were obtained as 7.7 nmol/mg of the expressed SERCA1a, 0.1 mM, and 1.6, respectively. The values presented are the mean ± S.D. (n = 7).

Stable Analog of Transient E2P with Occluded Ca²⁺ in SERCA

description and reasons for protection in [supplemental Fig. S5](#) and Ref. 56). By contrast, in mutant $E2Ca_2\cdot BeF_3^-$ and mutant $E2PCa_2$, the prtK-site Leu¹¹⁹ is rapidly cleaved and, thus, exposed. Evidently Leu¹¹⁹/Tyr¹²² on M2 in mutant $E2Ca_2\cdot BeF_3^-$ and mutant $E2PCa_2$ have moved from their hidden position in $E1PCa_2$ ($E1Ca_2\cdot BeF_3^-$) but are not yet buried again through interaction with the A and P domains as in $E2P$ ($E2\cdot BeF_3^-$), suggesting an intermediate structure. The results also reveal how critical the native length of the A/M1'-linker is for moving M2 and the A and P domains to realize the Ca²⁺-free state $E2P$ ($E2\cdot BeF_3^-$).

The proteolyses also reveal that wild type and mutant $E1Ca_2\cdot AlF_x$ are not structurally similar to wild type $E1Ca_2\cdot BeF_3^-$ ($E1PCa_2$) and mutant $E2Ca_2\cdot BeF_3^-$ ($E2PCa_2$). Interestingly, the rate of cleavage at the T2 site of mutant $E1Ca_2\cdot AlF_x$ is intermediate between that of wild type transition state ($E1Ca_2\cdot AlF_x/ E1Ca_2\cdot AlF_4^- \cdot ADP$) and that of the $E1PCa_2$ product state ($E1Ca_2\cdot BeF_3^-$), suggesting that the structure is also intermediate. Thus, elongation of the A/M1'-linker brought the $E1Ca_2\cdot AlF_x$ structure closer to that of wild type $E1Ca_2\cdot BeF_3^-$. Only BeF_x^- and not AlF_x^- produces a species analogous to the $E2PCa_2$ structural state ($E2Ca_2\cdot BeF_3^-$ via $E1Ca_2\cdot BeF_3^-$). This means that the phosphorylation reaction must have passed through the transition state to progress to the isomerization step.

In the mutant and wild type, the prtK-site Thr²⁴² on the A/M3-linker is completely resistant in all the states $E1Ca_2\cdot AlF_4^- \cdot ADP/ E1Ca_2\cdot AlF_x^-$, $E1Ca_2\cdot BeF_3^-$ ($E1PCa_2$), $E2Ca_2\cdot BeF_3^-$ and $E2PCa_2$, and $E2\cdot BeF_3^-/ E2\cdot AlF_4^-/ E2\cdot MgF_4^{2-}$ (as shown previously with sarcoplasmic reticulum Ca²⁺-ATPase (23, 24)). The result indicates that in both mutant and wild type, the A/M3-linker is strained by the A-domain rotation perpendicular to the membrane plane upon $E1PCa_2$ formation from $E1Ca_2$ and remains taut during EP processing.

$E2Ca_2\cdot BeF_3^-$ Formation from $E2\cdot BeF_3^-$ by Luminal Ca²⁺ Binding—The Ca²⁺-free complexes $E2\cdot BeF_3^-$, $E2\cdot AlF_4^-$, and $E2\cdot MgF_4^{2-}$ (the analogs of the $E2P$ ground state, transition state, and product complex of $E2P$ hydrolysis, respectively (25)) were first formed in mutant 4Gi-46/47 and wild type, with Mg²⁺ bound at the catalytic site, and subsequent proteolyses were performed with and without a 10 mM Ca²⁺ treatment in the presence of ionophore A23187 ([supplemental Fig. S4 and Table S2](#)). Under these conditions Ca²⁺-treated mutant $E2\cdot BeF_3^-$ exhibits complete resistance at the tryptic T2 site Arg¹⁹⁸ and a fairly rapid prtK cleavage at Leu¹¹⁹ on the top of M2, exactly as in mutant $E2PCa_2$ and $E2Ca_2\cdot BeF_3^-$ produced from $E1Ca_2$. These results agree with those in Fig. 3D where it is found that the ability to form EP is not restored by Ca²⁺ treatment of $E2\cdot BeF_3^-$. Thus, $E2Ca_2\cdot BeF_3^-$, as the $E2PCa_2$ analog, is produced from both $E2\cdot BeF_3^-$ and from $E1Ca_2$ (mimicking luminal Ca²⁺ binding to $E2P$ in the reverse direction of the pump cycle and the forward ATP-induced EP formation and isomerization, respectively). On the other hand, mutant and wild type complexes $E2\cdot AlF_4^-$ and $E2\cdot MgF_4^{2-}$ and wild type $E2\cdot BeF_3^-$ are destroyed by Ca²⁺ treatment as found previously with sarcoplasmic reticulum Ca²⁺-ATPase (25, 27).

Stability of Complex $E2Ca_2\cdot BeF_3^-$ —In Fig. 9, $E2Ca_2\cdot BeF_3^-$ was first produced from mutant $E1Ca_2$ with BeF_x^- in 50 μM ⁴⁵Ca²⁺ and 15 mM Mg²⁺, then further incubated at 25 °C in the pres-

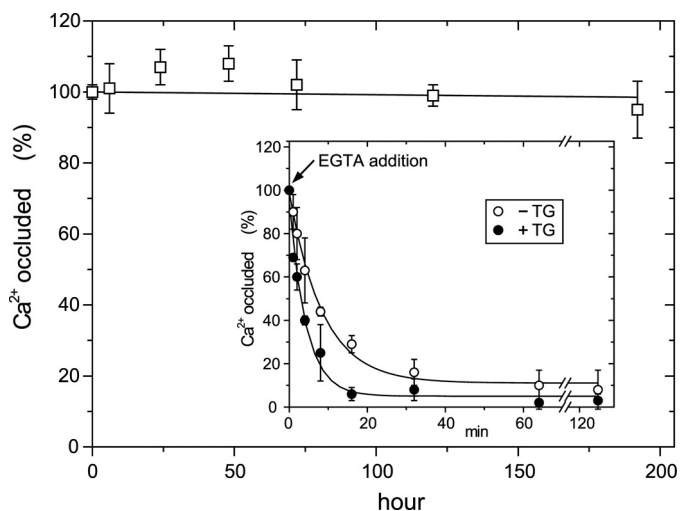


FIGURE 9. Stability of $E2Ca_2\cdot BeF_3^-$ of the mutant 4Gi-46/47. The complex $E2Ca_2\cdot BeF_3^-$ was produced with the mutant 4Gi-46/47 for 30 min at 25 °C in 0.05 mM ⁴⁵CaCl₂, 1 mM KF, 50 μM BeSO₄, and 15 mM MgCl₂ and otherwise as in Fig. 8A. Then a small volume of A23187 was added to give 1 μM, and the incubation was further continued at 25 °C. At various times, the amount of ⁴⁵Ca²⁺ specifically bound and occluded in the mutant was measured after an EGTA wash and by subtracting the background levels determined in the absence of F⁻ in the incubation mixture and otherwise as in Fig. 8A. *Inset*, after the formation of $E2Ca_2\cdot BeF_3^-$ as above, the sample was diluted 100-fold at 25 °C with a solution containing 1 μM A23187, 0.1 M KCl, 7 mM MgCl₂, 2 mM EGTA, and 50 mM MOPS/Tris (pH 7.0) (without BeF_x) in the absence (○) or presence (●) of 1 μM TG and incubated for various periods, and the amount of ⁴⁵Ca²⁺ specifically bound and occluded in the mutant was obtained as above. The values presented are the mean ± S.D. (*n* = 7). Solid lines in the *inset* show the least squares fit to a single exponential, and the decay rate constants thus obtained are 7.0 (○) and 14.0 (●) h⁻¹ without and with TG, respectively. In the *main panel* and *inset*, the amount of Ca²⁺ occluded in the complex $E2Ca_2\cdot BeF_3^-$ at time 0 (immediately before starting the long incubation or the dilution) was normalized to 100%.

ence of these ligands, and the amount of occluded ⁴⁵Ca²⁺ was determined. The results show that the complex $E2Ca_2\cdot BeF_3^-$ of the mutant is perfectly stable even after 1 week. Proteolysis confirms that the structure remains unchanged during the incubation (data not shown). The stability of the complex was further tested by diluting into an EGTA-containing solution without BeF_x, and the incubation was continued at 25 °C (see the *inset*). Ca²⁺ is slowly released with a rate constant of 7.0 h⁻¹. The addition of thapsigargin (TG) to the diluent only doubles the rate of release, indicating that the transmembrane domain is fairly resistant to TG-induced structural perturbation. These decay rates are very similar to those of mutant $E2PCa_2$ without and with TG addition, 9.7 and 27.3 h⁻¹, respectively (14). Thus, in this respect also, mutant $E2Ca_2\cdot BeF_3^-$ is analogous to mutant $E2PCa_2$.

DISCUSSION

Mutant $E2Ca_2\cdot BeF_3^-$ as an Analog of Native Transient State $E2PCa_2$ —Using our elongated A/M1'-linker mutant, we have developed the complex $E2Ca_2\cdot BeF_x^-$, most probably $E2Ca_2\cdot BeF_3^-$, as a stable structural analog of the native transient state $E2PCa_2$ (ADP-insensitive EP with two Ca²⁺ at the transport sites), an intermediate in EP isomerization and Ca²⁺ deocclusion/release. The complex $E2Ca_2\cdot BeF_3^-$ has two occluded Ca²⁺ and is produced from both mutant $E1Ca_2$ and mutant $E2\cdot BeF_3^-$, mimicking native $E2PCa_2$ formation from $E1Ca_2$ after ATP-induced forward phosphorylation via $E1PCa_2$ isomerization

and in the reverse direction from E2P after luminal Ca²⁺ binding. Mutant E2Ca₂·BeF₃⁻ formation requires Mg²⁺ at the catalytic site as in native ATP- and P_i-induced EP formation. The disposition of the cytoplasmic domains in mutant E2Ca₂·BeF₃⁻ is equivalent to that in E2PCa₂ trapped with the mutant and intermediate between native E1PCa₂·Mg²⁺ (E1Ca₂·BeF₃⁻ of wild type) and native E2P·Mg²⁺ (E2·BeF₃⁻ of wild type and mutant). All these properties of mutant E2Ca₂·BeF₃⁻ meet the requirements of a native E2PCa₂ analog.

Importantly, AlF_x and MgF_x are not able to produce this E2PCa₂ analog either from mutant E1Ca₂ or from mutant E2·AlF₄⁻ and E2·MgF₄²⁻. Thus, BeF_x is unique in this regard. The coordination chemistry of the beryllium in BeF_x (BeF₃⁻) allows it to directly ligate the aspartyl oxygen, thereby producing the same tetrahedral geometry as the covalent Asp³⁵¹-acylphosphate, as seen in the atomic structure of the E2P ground state analog E2·BeF₃⁻ (21, 22). On the other hand, AlF_x (AlF₃ or AlF₄⁻) mimics the transition state of phosphorylation and dephosphorylation as seen in structures E1Ca₂·AlF₄⁻·ADP and E2·AlF₄⁻ (17, 19, 22). MgF₄²⁻ mimics P_i in the product complex E2·P_i after E2P hydrolysis as seen in structure E2·MgF₄²⁻ (19). Our results taken together with the coordination chemistry show that the structural changes for EP isomerization and Ca²⁺ deocclusion/release in the forward and reverse reactions are strictly coupled with the particular configuration of the acylphosphate after formation of the covalent bond within the catalytic site. The product E1PCa₂ state and the E2P ground state are ready for the changes, but the transition state structures are not.

Roles of A/M1'-linker and Structural Changes during EP Formation and Processing—The transient E2PCa₂ state formed during EP processing and its analog E2Ca₂·BeF₃⁻ were trapped and stabilized by elongation of the A/M1'-linker. As revealed by the proteolyses, in mutant E2Ca₂·BeF₃⁻ and mutant E2PCa₂, the A domain has already rotated parallel to membrane from its position in E1Ca₂·BeF₃⁻ (E1PCa₂·Mg) and has associated with the P domain at the Val²⁰⁰ loop. Because mutant E2PCa₂ is ADP-insensitive (14), the outermost loop TGES¹⁸⁴ of the A domain is most probably docked onto the Asp³⁵¹ region, thereby blocking ADP access to the Asp³⁵¹ acylphosphate (19). Thus, in mutant E2Ca₂·BeF₃⁻ and mutant E2PCa₂, the A domain is positioned above the P domain. On the other hand, the proteolyses also show that the spatial relationship of the top part of M2 (Leu¹¹⁹/Tyr¹²²) with the P and A domains in mutant E2Ca₂·BeF₃⁻ (equivalent to native E2PCa₂·Mg) is intermediate between those of the wild type E1Ca₂·BeF₃⁻ (native E1PCa₂·Mg) and the wild type and mutant E2·BeF₃⁻ (native E2P·Mg). Thus, Leu¹¹⁹ (the prtK site) on the top part of M2 has broken its van der Waals contact with upper M4 seen in E1PCa₂ but has not yet reached the P and A domains to form their interaction network at Leu¹¹⁹/Tyr¹²², *i.e.* the Tyr¹²² hydrophobic cluster has not formed (see supplemental Fig. S5 for its structure). This interaction network formed from Ile¹⁷⁹/Leu¹⁸⁰/Ile²³² of the A domain, Val⁷⁰⁵/Val⁷²⁶ of the P domain, and Tyr¹²²/Leu¹¹⁹ of M2 is actually critical for the E2P structure (11–13). Therefore, in E2Ca₂·BeF₃⁻ and E2PCa₂ stabilized by elongation of the A/M1'-linker, the inclining motions of

domains and helix are not yet advanced enough to reach the E2P structure.

Deletion of any single residue in the A/M1'-linker, *i.e.* shortening it, completely blocks E1PCa₂ isomerization to E2PCa₂ (26). By contrast, its elongation markedly accelerates the isomerization and greatly stabilizes E2PCa₂ blocking Ca²⁺ deocclusion/release from this transient state (14). These findings suggest that formation of the transient E2PCa₂ state (mutant E2Ca₂·BeF₃⁻) from E1PCa₂ (E1Ca₂·BeF₃⁻), strains the A/M1'-linker with the wild type/native length due to rotation and positioning of the A domain above the P domain, which in turn causes further movements of the A and P domains facilitating Ca²⁺ deocclusion/release (14) (see the schematic model in supplemental Fig. S6). The A and P domains incline more, as will M1/M2 and M4/M5 connected with these domains, favoring release of the Ca²⁺. This view agrees with the structural changes required for Ca²⁺ release described by Toyoshima *et al.* (19); the bending and movement of M4/M5 by inclination of the P domain is predicted to destroy the Ca²⁺ binding sites, and the inclination of M2 and M1 (as a V-shaped rigid body) will push the lower part of M4 via M1 and open the luminal gate.

These domain and segmental motions associated with Ca²⁺ release will establish the interaction network at Leu¹¹⁹/Tyr¹²², the Tyr¹²² hydrophobic cluster, and stabilize the E2P structure with the luminal gate open (11–13). The position of the two A-P domain interaction networks, with Leu¹¹⁹/Tyr¹²² at the lower part and Val²⁰⁰ loop on the upper part of the interface, seems particularly appropriate to stabilize the inclined A and P domains and helices and, therefore, the gate in an open state.

These cluster formations are also critical for producing the E2P catalytic site with hydrolytic ability (11–13). Therefore, in this mechanism E2P hydrolysis can only occur after Ca²⁺ release, ensuring energy coupling. The relative stability of native E2P may function as a brake to allow enough time for releasing Ca²⁺ and for refining the catalytic site for subsequent hydrolysis, *e.g.* appropriate positioning of TGES¹⁸⁴ and Glu¹⁸³-coordinated attacking water molecule.

Ca²⁺ Substitution of Mg²⁺ at the Catalytic Site—In the elongated A/M1'-linker mutant, Ca²⁺ as well as Mg²⁺ bound at the catalytic Mg²⁺ site is able to produce E2Ca₂·BeF₃⁻ from E1Ca₂ via E1Ca₂·BeF₃⁻. This binding of Ca²⁺ is also found when mutant E2PCa₂ is formed from CaATP in the absence of Mg²⁺ (14). This is in sharp contrast to the situation in the wild type, where Ca²⁺ cannot substitute for Mg²⁺ at the catalytic site for E1Ca₂·BeF₃⁻ formation. An attempt to substitute Ca²⁺ for Mg²⁺ actually destroys wild type E1Ca₂·BeF₃⁻ (27). The extremely rapid isomerization of EP with bound Ca²⁺ at the Mg²⁺ site in the elongated A/M1'-linker mutant (E1PCa₂·Ca → E2PCa₂·Ca) is again very different to the markedly retarded E1PCa₂·Ca isomerization in wild type (14). The atomic structures provide insights into why elongation of the linker allows Ca²⁺ to replace Mg²⁺ at the catalytic site.

In the atomic structures of E1Ca₂·CaAMPPCP and E1Ca₂·AlF₄⁻·ADP described by Toyoshima *et al.* (18, 19), Mg²⁺ or Ca²⁺ ligation at the catalytic Mg²⁺ site I (Asp³⁵¹/Thr³⁵³/Asp⁷⁰³ of the P domain and the phosphate moiety (or its analog); see Fig. 2) induces the P domain to bend and, thereby, the A domain to rotate upward, perpendicular to the membrane plane (see

Stable Analog of Transient E2P with Occluded Ca²⁺ in SERCA

Figs. 4 and 5 in Ref. 18 and the schematic in [supplemental Fig. S6](#)). This A-domain rotation raises its junctions with the A/M1'-linker and the A/M3-linker. The strain imposed on the A/M3-linker in E1PCa₂ probably drives the large horizontal rotation of the A domain during E1PCa₂ to E2P isomerization (18, 19, 50, 51). In the stringent coordination chemistry, the ligation length is shorter in Mg²⁺ than in Ca²⁺ typically by 0.2 Å (e.g. 2.1 versus 2.3 Å (52, 53)). Therefore, Mg²⁺ ligation probably induces more P-domain bending and in consequence more upward swinging of the A domain, leading to a stronger pull from the A/M3-linker to effect the horizontal rotation of the A domain (27). This is substantiated by the finding that in wild type, E1PCa₂·Mg²⁺ is rapidly isomerized, whereas in E1PCa₂·Ca it is markedly retarded (28, 29).

The observed formation of E2Ca₂·BeF₃⁻ and E2PCa₂ (via very rapid E1PCa₂ isomerization) from mutant E1Ca₂ with Ca²⁺ or Mg²⁺ at the catalytic Mg²⁺ site shows that the poor Ca²⁺ effect on the A-domain upward rotation and subsequent horizontal rotation is relieved by elongation of the A/M1'-linker. Note again that the A-domain junction with the A/M1'-linker is raised by the upward movement of the A domain. It is, therefore, likely that in wild type, the A/M1'-linker is strained to some extent by this movement of the A domain on formation of E1PCa₂. This possible strain is evidently not deleterious for wild type, but it becomes a serious energy barrier when the A/M1'-linker is shortened by deletion of any single residue as the deletions completely block E1PCa₂ to E2PCa₂ isomerization (26). Strain in the wild type A/M1'-linker in E1PCa₂ is likely to be important as a build up to generating stronger strain during E1PCa₂ to E2PCa₂ isomerization. Thus, the strain of the A/M1'-linker seems to be imposed increasingly during E1PCa₂ formation and the subsequent isomerization to E2PCa₂, and this energy finally could be used for inducing structural changes for Ca²⁺ deocclusion and release.

E1Ca₂·AlF_x Formed from E1Ca₂ in the Elongated A/M1'-linker Mutant—The proteolytic analyses reveal that in wild type organization of the cytoplasmic domains of the transition state analog E1Ca₂·AlF_x is identical to that of E1Ca₂·AlF₄⁻·ADP and has obviously not yet reached the product E1PCa₂ state E1Ca₂·BeF₃⁻. Namely, during the reaction E1Ca₂·AlF₄⁻·ADP/E1Ca₂·AlF_x → E1Ca₂·BeF₃⁻, the A domain rotates partially in a horizontal direction and comes close to the P domain at tryptic T2 site Arg¹⁹⁸ but is not completely engaged, so that it cannot produce the E2Ca₂·BeF₃⁻ and E2·BeF₃⁻ states (Ref. 27 and see the schematic in [supplemental Fig. S6](#)). On the other hand, in the elongated A/M1'-linker mutant, the structure of E1Ca₂·AlF_x is intermediate between those of E1Ca₂·AlF₄⁻·ADP and E1Ca₂·BeF₃⁻ of wild type as judged from the intermediate tryptic cleavage rate at Arg¹⁹⁸. Thus, elongation of the A/M1'-linker partly relieves barriers to A-domain rotation, bringing the structure of E1Ca₂·AlF_x closer to that of E1Ca₂·BeF₃⁻. The finding agrees with our above postulate that the A/M1'-linker is strained by the A-domain upward movement during E1PCa₂ (E1Ca₂·BeF₃⁻) formation from the transition state (E1Ca₂·AlF_x). In fact, because the length of the Asp³⁵¹ O-phosphate bond in the transition state (as mimicked by AlF_x) is obviously longer than that of the covalent acylphosphate bond (as mimicked by BeF₃⁻), the transition state (AlF_x) must exhibit less P-domain bending.

Luminal Ca²⁺-induced E2Ca₂·BeF₃⁻ Formation from E2·BeF₃⁻—The observed reverse formation of E2Ca₂·BeF₃⁻ (native E2PCa₂) from mutant E2·BeF₃⁻ (E2P) through Ca²⁺ binding from the lumen shows that the luminal gate (Ca²⁺ releasing pathway) is open in E2·BeF₃⁻ (E2P ground state immediately before Ca²⁺ binding). This is in contrast to the closed gate in E2·AlF₄⁻ and E2·MgF₄²⁻ (25). Thus, luminal gating is strictly coupled with the configuration change in the phosphate during E2P hydrolysis, thereby avoiding possible Ca²⁺ leakage (25). Note that in wild type, E2·BeF₃⁻ (open luminal gate) formed with Mg²⁺ is converted to E1Ca₂ + BeF_x by Ca²⁺, because cycle reversal and subsequent Ca²⁺ substitution of Mg²⁺ at the catalytic site destabilizes E1Ca₂·BeF₃⁻ as previously demonstrated (27). E2·AlF₄⁻ and E2·MgF₄²⁻ (gates closed) in wild type and mutant were also decomplexed to E1Ca₂ by Ca²⁺ but probably by the high Ca²⁺ concentration disrupting the luminal and transmembrane regions, thereby destabilizing AlF₄⁻ and MgF₄²⁻ ligation at the catalytic site.

Mg²⁺ Dependence of E2Ca₂·BeF₃⁻ Formation from E1Ca₂—The Mg²⁺ as well as Mn²⁺ or Ca²⁺ dependence of E2Ca₂·BeF₃⁻ formation from mutant E1Ca₂ (Fig. 5 and [supplemental Figs. S1 and S2](#)) exhibited a Hill coefficient of 2, which is in contrast to the value of 1 for wild type E1Ca₂·BeF₃⁻ formation from E1Ca₂ (27). The results suggest that one or more Mg²⁺ besides the one at catalytic Mg²⁺ site I is involved cooperatively in the E2Ca₂·BeF₃⁻ formation from E1Ca₂. In the atomic structures of E1Ca₂·CaAMPPCP and E1Ca₂·AlF₄⁻·ADP, only one Mg²⁺ (or Ca²⁺) at site I is seen (in addition to the one coordinated with the nucleotide, which was predicted to aid phosphoryl transfer). Also, in the structures of E2·BeF₃⁻, E2·AlF₄⁻, and E2·MgF₄²⁻, only one Mg²⁺ is seen (at site I). Therefore, in E2Ca₂·BeF₃⁻ (E2PCa₂) formation a second (or more) Mg²⁺ may possibly be required only transiently and, together with the catalytic ion, aids the motions of N, P, and A domains and their gathering during the E1PCa₂ isomerization to E2PCa₂.

In summary, our previous (14, 26) and present studies show that the A/M1'-linker should be appropriately long for the E1PCa₂ to E2PCa₂ isomerization then short enough for the Ca²⁺ deocclusion/release from E2PCa₂ and again appropriately long for E2P hydrolysis. Thus, the length of the A/M1'-linker in wild type is naturally designed to induce successive structural changes and motions of the cytoplasmic and transmembrane domains for these processes. These functions of the A/M1'-linker act in concert with the changing configuration of the phosphate and catalytic Mg²⁺ and the Asp³⁵¹-phosphate bond length, with strength being critical in the formation of E2PCa₂, a species poised to deliver Ca²⁺ to the lumen. The stable analogs, E1Ca₂·BeF₃⁻ (27) and E2Ca₂·BeF₃⁻ (this study) with bound Mg²⁺ could be critically important for obtaining atomic models of E1PCa₂·Mg²⁺ and the hitherto elusive transient E2PCa₂·Mg²⁺ intermediate for further understanding of the transport mechanism.

Acknowledgments—We thank Dr. David H. MacLennan, University of Toronto, for the generous gift of SERCA1a cDNA and Dr. Randal J. Kaufman, Genetics Institute, Cambridge, MA, for the generous gift of the expression vector pMT2. We are also grateful to Dr. Chikashi Toyoshima, University of Tokyo, for helpful discussions. We thank Dr. David B. McIntosh for reviewing and improving our manuscript.

REFERENCES

- Hasselbach, W., and Makinose, M. (1961) *Biochem. Z.* **333**, 518–528
- Ebashi, S., and Lipmann, F. (1962) *J. Cell Biol.* **14**, 389–400
- Inesi, G., Sumbilla, C., and Kirtley, M. E. (1990) *Physiol. Rev.* **70**, 749–760
- Møller, J. V., Juul, B., and le Maire, M. (1996) *Biochim. Biophys. Acta* **1286**, 1–51
- MacLennan, D. H., Rice, W. J., and Green, N. M. (1997) *J. Biol. Chem.* **272**, 28815–28818
- McIntosh, D. B. (1998) *Adv. Mol. Cell Biol.* **23**, 33–99
- Toyoshima, C., and Inesi, G. (2004) *Annu. Rev. Biochem.* **73**, 269–292
- Toyoshima, C. (2008) *Arch. Biochem. Biophys.* **476**, 3–11
- Toyoshima, C. (2009) *Biochim. Biophys. Acta* **1793**, 941–946
- Kato, S., Kamidochi, M., Daiho, T., Yamasaki, K., Gouli, W., and Suzuki, H. (2003) *J. Biol. Chem.* **278**, 9624–9629
- Yamasaki, K., Daiho, T., Danko, S., and Suzuki, H. (2004) *J. Biol. Chem.* **279**, 2202–2210
- Wang, G., Yamasaki, K., Daiho, T., and Suzuki, H. (2005) *J. Biol. Chem.* **280**, 26508–26516
- Yamasaki, K., Wang, G., Daiho, T., Danko, S., and Suzuki, H. (2008) *J. Biol. Chem.* **283**, 29144–29155
- Daiho, T., Yamasaki, K., Danko, S., and Suzuki, H. (2007) *J. Biol. Chem.* **282**, 34429–34447
- Toyoshima, C., Nakasako, M., Nomura, H., and Ogawa, H. (2000) *Nature* **405**, 647–655
- Toyoshima, C., and Nomura, H. (2002) *Nature* **418**, 605–611
- Sørensen, T. L., Møller, J. V., and Nissen, P. (2004) *Science* **304**, 1672–1675
- Toyoshima, C., and Mizutani, T. (2004) *Nature* **430**, 529–535
- Toyoshima, C., Nomura, H., and Tsuda, T. (2004) *Nature* **432**, 361–368
- Olesen, C., Sørensen, T. L., Nielsen, R. C., Møller, J. V., and Nissen, P. (2004) *Science* **306**, 2251–2255
- Toyoshima, C., Norimatsu, Y., Iwasawa, S., Tsuda, T., and Ogawa, H. (2007) *Proc. Natl. Acad. Sci. U.S.A.* **104**, 19831–19836
- Olesen, C., Picard, M., Winther, A. M., Gyrupe, C., Morth, J. P., Oxvig, C., Møller, J. V., and Nissen, P. (2007) *Nature* **450**, 1036–1042
- Danko, S., Daiho, T., Yamasaki, K., Kamidochi, M., Suzuki, H., and Toyoshima, C. (2001) *FEBS Lett.* **489**, 277–282
- Danko, S., Yamasaki, K., Daiho, T., Suzuki, H., and Toyoshima, C. (2001) *FEBS Lett.* **505**, 129–135
- Danko, S., Yamasaki, K., Daiho, T., and Suzuki, H. (2004) *J. Biol. Chem.* **279**, 14991–14998
- Daiho, T., Yamasaki, K., Wang, G., Danko, S., Iizuka, H., and Suzuki, H. (2003) *J. Biol. Chem.* **278**, 39197–39204
- Danko, S., Daiho, T., Yamasaki, K., Liu, X., and Suzuki, H. (2009) *J. Biol. Chem.* **284**, 22722–22735
- Shigekawa, M., Wakabayashi, S., and Nakamura, H. (1983) *J. Biol. Chem.* **258**, 8698–8707
- Wakabayashi, S., and Shigekawa, M. (1987) *J. Biol. Chem.* **262**, 11524–11531
- Kaufman, R. J., Davies, M. V., Pathak, V. K., and Hershey, J. W. B. (1989) *Mol. Cell. Biol.* **9**, 946–958
- Maruyama, K., and MacLennan, D. H. (1988) *Proc. Natl. Acad. Sci. U.S.A.* **85**, 3314–3318
- Daiho, T., Yamasaki, K., Suzuki, H., Saino, T., and Kanazawa, T. (1999) *J. Biol. Chem.* **274**, 23910–23915
- Murphy, A. J., and Coll, R. J. (1992) *J. Biol. Chem.* **267**, 5229–5235
- Troullier, A., Girardet, J. L., and Dupont, Y. (1992) *J. Biol. Chem.* **267**, 22821–22829
- Murphy, A. J., and Coll, R. J. (1993) *J. Biol. Chem.* **268**, 23307–23310
- Kubota, T., Daiho, T., and Kanazawa, T. (1993) *Biochim. Biophys. Acta* **1163**, 131–143
- Weber, K., and Osborn, M. (1969) *J. Biol. Chem.* **244**, 4406–4412
- Daiho, T., Suzuki, H., Yamasaki, K., Saino, T., and Kanazawa, T. (1999) *FEBS Lett.* **444**, 54–58
- Laemmli, U. K. (1970) *Nature* **227**, 680–685
- Lowry, O. H., Rosebrough, N. J., Farr, A. L., and Randall, R. J. (1951) *J. Biol. Chem.* **193**, 265–275
- Humphrey, W., Dalke, A., and Schulten, K. (1996) *J. Mol. Graph.* **14**, 33–38
- de Meis, L., and Masuda, H. (1974) *Biochemistry* **13**, 2057–2062
- Masuda, H., and de Meis, L. (1973) *Biochemistry* **12**, 4581–4585
- Hasselbach, W., Fassold, E., Migala, A., and Rauch, B. (1981) *Fed. Proc.* **40**, 2657–2661
- González, D. A., Ostuni, M. A., Lacapère, J. J., and Alonso, G. L. (2006) *Biophys. Chem.* **124**, 27–34
- Yamada, S., and Ikemoto, N. (1980) *J. Biol. Chem.* **255**, 3108–3119
- Kanazawa, T. (1975) *J. Biol. Chem.* **250**, 113–119
- Ogurusu, T., Wakabayashi, S., and Shigekawa, M. (1991) *J. Biochem.* **109**, 472–476
- de Meis, L., and Inesi, G. (1982) *J. Biol. Chem.* **257**, 1289–1294
- Møller, J. V., Lenoir, G., Marchand, C., Montigny, C., le Maire, M., Toyoshima, C., Juul, B. S., and Champeil, P. (2002) *J. Biol. Chem.* **277**, 38647–38659
- Holdensen, A. N., and Andersen, J. P. (2009) *J. Biol. Chem.* **284**, 12258–12265
- Picard, M., Jensen, A. M., Sørensen, T. L., Champeil, P., Møller, J. V., and Nissen, P. (2007) *J. Mol. Biol.* **368**, 1–7
- Peeraer, Y., Rabijns, A., Collet, J. F., Van Schaftingen, E., and De Ranter, C. (2004) *Eur. J. Biochem.* **271**, 3421–3427
- Juul, B., Turc, H., Durand, M. L., Gomez de Gracia, A., Denoroy, L., Møller, J. V., Champeil, P., and le Maire, M. (1995) *J. Biol. Chem.* **270**, 20123–20134
- Lenoir, G., Picard, M., Gauron, C., Montigny, C., Le Maréchal, P., Falson, P., Le Maire, M., Møller, J. V., and Champeil, P. (2004) *J. Biol. Chem.* **279**, 9156–9166
- Seekoe, T., Peall, S., and McIntosh, D. B. (2001) *J. Biol. Chem.* **276**, 46737–46744